Functional Connectome Prediction of Anxiety Related to the COVID-19 Pandemic

He, L., Wei, D., Yang, F., et al (2021)

Supplementary Material

American Journal of Psychiatry DOI: 10.1176/appi.ajp.2020.20070979

Method S1. Participants

For the three undergraduate datasets, we used stringent inclusion and exclusion criteria to ensure that all participants had no psychiatric illness or physical health problems and met the requirements for MRI scanning. Specifically, all students of the Southwest University undertook standardized physical examinations at the affiliated hospital of the Southwest University and all participants from the three datasets had passed the examination, and no one reported major physical illness before the brain scanning. Meanwhile, a well-trained and experienced research assistant performed a Structured Clinical Interview based on the DSM-IV for each participant to ensure participants had no current or prior history of psychiatric disorders or neurological illness and were not taking psychoactive medications (e.g., antidepressant drugs) that might affect brain function. In addition, participants met the safety requirement for MRI scanning, the exclusion criteria including claustrophobia, metallic implants, pregnancy, and a history of head trauma and fainting. For the concerns of excessive head motion during the brain scanning and to ensure that head motion artefacts were not driving observed effects, we adopted a widely used criterion to exclude participants based on > 10% bad volumes (1-3). The bad time points were defined as volumes with framewise displacement (FD) Power > 0.5 mm as well as the two succeeding volumes and one preceding volume to reduce the spillover effect of head motion (1-3).

All recruited participants from the three undergraduate datasets were freshmen or sophomores fluent in Chinese to ensure sample homogeneity, which also helped the longitudinal survey while at the university. The BBP is our ongoing project that began in Sep 2019, which aims to explore the neural basis of Chinese personality and trait-like behaviours. The SLIM cohort was initiated in November 2011 and finished in January 2015, which included multimodal MRI data and various behavioral variables at three time points (4). The average number of days between the first scan and the third scan are 817.87 days. Considering that the first time point of the SLIM includes the largest sample size, we used the first time point data of the SLIM that were collected from November 2011 to January 2013, which included 474 participants who

both completed brain scanning and anxiety measures after excluding 12 participants with excessive head motion.

All participants' anxiety scores of the three undergraduate datasets were measured by the State-Trait Anxiety Inventory (STAI) (5). For the BBP and SLIM, participants completed the STAI and other emotional questionnaires immediately after the brain scanning. Notably, the BBP participants had only completed the trait section of the STAI because the initial design mainly focused on personality and trait-related behavioural and psychological variables. The validation sample was initially designed to explore the relation between creativity, semantic cognition, associative abilities, and executive functions by combining brain structural and functional images, and participants of the validation sample had not completed anxiety-related questionnaires after the brain scanning.

During the COVID-19 pandemic, a total of 901 undergraduates from the BBP were recruited via mobile phone text-message to complete the first online pandemic questionnaire survey from February 22 to 28, 2020. Among them, 604 participants had completed pre-pandemic brain scanning from September to December 2019 and a self-reported anxiety measurement immediately after the scanning (considered as baseline or daily anxiety), in which 8 participants missed baseline anxiety measurement, and 7 participants were excluded due to excessive head motion. Thus, for the first pandemic survey of the BBP, 589 undergraduates with brain imaging data, baseline anxiety, and pandemic-related anxiety were included in predictive analysis to examine the prediction from the functional connectome of daily anxiety and pandemic-related anxiety, and to identify the connectome-based neuromarkers of pandemic-related anxiety. The SLIM was used to validate the predictions from the functional connectome of daily anxiety. Some participants (486 undergraduates) from the BBP had also completed the second online pandemic questionnaire survey from April 24 to May 1, 2020. In addition, a validation sample included 149 undergraduates who had completed an online pandemic questionnaire survey from February 21 to 28, 2020 and brain scanning from June to October 2019, in which no one was excluded due to excessive head motion. The validation sample and the

anxiety score from the second pandemic survey of the BBP were used to examine the reliability of the neural correlates of pandemic-related anxiety identified in the first pandemic survey.

In addition, we further explored the clinical relevance of the connectome-based neuromarkers of pandemic-related anxiety by linking them to different mental disorders. Details on clinical diagnosis and symptom information for each dataset can be found in previous studies (3, 6-9).

Generalized Anxiety. Initially, 1885 participants were recruited via advertisement and school posters from local senior high schools in Hunan Province, China (7). The Screen for Child Anxiety Related Emotional Disorders (SCARED) was used for preliminary screening. Participants with a SCARED score ≥ 25 were considered as potential individuals with anxiety disorders (10, 11). There were 508 participants with SCARED score ≥ 25, and 1377 participants with SCARED score < 25 (165 participants were randomly selected from the low-score group used in the next step). Next, 673 participants, including 508 adolescents with SCARED score ≥ 25, and 165 adolescents with SCARED scores < 25 were interviewed and diagnosed by trained clinicians. The diagnosis protocol was established based on the Schedule for Affective Disorders and Schizophrenia for School-Age Children-Present and Lifetime version, which was conducted independently by one certified pediatric psychiatrist according to the DSM-IV criteria (12). Inclusion criteria for generalized anxiety included: current first-episode, medication-naive generalized anxiety; without comorbidity; and between the ages of 13–18 years old. HCs were recruited according to the following criteria: no personal or family history of psychosis; no pervasive developmental disorder, intellectual disability, Tourette's syndrome, conduct disorder, bipolar disorder, mania, current major depression, other kinds of anxiety disorders, psychotic disorder, history of head injury or seizures, and alcohol and substance abuse. All participants in the current study were right-handedness and had normal full-scale IQ (> 80) as measured by the Wechsler Abbreviated Scale of Intelligence (13). Finally, 36 participants with generalized anxiety and 28 HCs completed brain imaging scanning. After excluding participants with excessive head motion, the final sample included 24

participants with generalized anxiety and 18 HCs. This research protocol was approved by the local Medical Ethics Committee in the Second Xiangya Hospital of Central South University, China. Written informed consents were obtained from parents or legal guardians of all participants in accordance with the Declaration of Helsinki.

Major Depression. The second sample included 282 participants with major depression and 254 HCs from the First Affiliated Hospital of Chongqing Medical School and Southwest University (3). Participants with major depression were recruited from the outpatient department of the First Affiliated Hospital of Chongqing Medical School in Chongqing, China. All were diagnosed according to the Structured Clinical Interview for DSM-IV (SCID), by independent assessments of two psychiatrists. The patient would not be included in the dataset if any psychiatrist diagnosed the patient as non-major depression. That is, all patients in the dataset were diagnosed with major depression by both psychiatrists. They were also assessed for disease severity using the Hamilton Depression Rating Scale and Beck Depression Inventory, illness duration and the medication status of the patients. Before the investigation, we excluded individuals who were not suitable for MRI scanning by interview and by the self-reported checklist. The MRI related exclusion criteria included claustrophobia, metallic implants, pregnancy, Meniere's Syndrome, and a history of fainting within the previous half year. Exclusion criteria for both groups were as follows: current psychiatric disorders (except for major depression) and neurological disorders, substance abuse, and stroke or serious encephalopathy. Of note, all of the subjects in the control group did not meet DSM-IV criteria for any psychiatric disorders and did not use any drugs that could affect brain function. The final sample included 282 participants with major depression and 254 HCs. No one was excluded due to excessive head motion. This research protocol was approved by the Research Ethics Committee of the Brain Imaging Center of Southwest University and the First Affiliated Hospital of Chongqing Medical School. Informed written consent was obtained from each subject in accordance with the Declaration of Helsinki.

Schizophrenia. The third sample included 72 participants with schizophrenia and 75 HCs from the Center of Biomedical Research Excellence and the raw data can be download from the International Neuroimaging Data-sharing Initiative (http://fcon_1000.projects.nitrc.org/indi/retro/cobre.html). The patients with a chronological age of 18–65 years were recruited from the outpatient clinic at the University of New Mexico Health Sciences Center. Participants were administered the SCID to verify their diagnoses of schizophrenia, with no other psychiatric dysfunction within the last 12 months. Exclusion criteria for patients with schizophrenia included a history of neurological disorder, head trauma with loss of consciousness greater than 5 min, mental retardation, active substance dependence or abuse (except for nicotine) within the past year, current use of mood stabilizers, history of dependence on PCP, amphetamines or cocaine, or history of PCP, amphetamine, or cocaine use within the last 12 months. HCs also received the SCID-non-patient edition to rule out axis I conditions in order to determine that they had no psychiatric dysfunction. Exclusion criteria included current or past psychiatric disorder, family history of a psychotic disorder in a first-degree relative, history of neurological disorder, head trauma with a loss of consciousness greater than 5 min, mental retardation, recent history of substance abuse or dependence, history of more than one lifetime depressive episode, history of depression or antidepressant use within the last 6 months, and history of lifetime antidepressant use of more than 1 year. After excluding participants with excessive head motion, the final sample included 26 participants with schizophrenia and 46 HCs. This research protocol was approved by the University of New Mexico Health Sciences Center Human Research Review Committee and complied with the Declaration of Helsinki. All participants provided written informed consent prior to study procedures.

Method S2. Neuroimaging Data Acquisition and Preprocessing

The three undergraduate datasets and the major depression dataset were collected from the Brain Imaging Center of the Southwest University, China. The generalized

anxiety dataset was collected from the Second Xiangya Hospital of Central South University, China. The schizophrenia dataset was collected from the University of New Mexico.

For the BBP and the validation sample, the brain imaging data was collected on a 3T Prisma Siemens Trio MRI scanner (Siemens Medical Systems, Erlangen, Germany) using a 32-chanel brain coil at Southwest University Brain Imaging Center. Resting-state fMRI data was obtained with gradient echo-planar imaging (EPI) sequence: repetition time (TR) = 2,000 ms, echo time (TE) = 30 ms, field of view (FOV) = 224 × 224, flip angle (FA) = 90°, slices = 62, thickness = 2 mm, slice gap = 0.3 mm, voxel size = 2 × 2 × 2 mm^3. This scanning contained 240 volumes. All participants were instructed to close their eyes and rest but not to fall asleep. High-resolution T1-weighted structural images were acquired using a magnetization prepared rapid acquisition gradient-echo (MPRAGE) sequence: TR = 2530 ms, TE = 2.98 ms, FOV = 224 × 256 mm^2, resolution matrix = 448 × 512, flip angle = 7°, slices = 192, thickness = 1.0 mm, inversion time = 1100 ms, voxel size = 0.5 × 0.5 × 1 mm^3.

For the SLIM (4) and major depression datasets (3), brain imaging data was collected on a 3T Siemens scanner (Siemens Medical Systems, Erlangen, Germany) using a 12-chanel brain coil at Southwest University Brain Imaging Center. Resting-state fMRI data was obtained using EPI sequence: TR = 2,000 ms, echo TE = 30 ms, FOV = 224 × 224, FA = 90°, slices = 32, thickness = 3 mm, slice gap = 1 mm, voxel size = 3.4 × 3.4 × 3 mm^3. This scanning contained 242 volumes. All participants were instructed to close their eyes and rest but not to fall asleep. High-resolution T1-weighted structural images were acquired using a MPRAGE sequence: TR = 1900 ms, TE = 2.52 ms, resolution matrix = 256 × 256, flip angle = 9°, slices = 176, thickness = 1.0 mm, inversion time = 900 ms, voxel size = 1 × 1 × 1 mm^3.

For the generalized anxiety dataset (7), brain imaging data was acquired using a Philips 3.0 Tesla scanner with a SENSE-8 channel head coil. Participants were instructed to relax, keep their heads still, eyes closed, and think of nothing during the MRI scanning procedure. The resting state functional images were obtained using gradient recalled echo planar imaging (GRE-EPI) with the following parameters: TR

= 3000 ms; TE = 30 ms; FA = 90◦; slice thickness = 4 mm; FOV = 240 mm × 240 mm; 36 trans-axial slices with no gap. This scanning contained 180 volumes. T1-weighted data were obtained using 3D rapid acquisition gradient echo sequence with the following parameters: TR = 7.5 ms; TE = 3.7 ms; flip angle = 8°; FOV = 256 mm × 256 mm; slices = 180; voxel size = 1 × 1 × 1 mm^3; axial slices.

For the schizophrenia dataset (http://fcon_1000.projects.nitrc.org/indi/retro/cobre.html), resting-state functional brain imaging data was collected with single-shot full k-space echo-planar imaging (EPI) with ramp sampling correction using the intercomissural line (AC-PC) as a reference: TR = 2 s, TE = 29 ms, matrix size = 64 × 64, slices = 32, voxel size = 3 × 3 × 4 mm^3. This scanning contained 150 volumes. T1-weighted structural images were acquired using a multi-echo MPRAGE (MEMPR) sequence with the following parameters: TR/TE/TI = 2530/[1.64, 3.5, 5.36, 7.22, 9.08]/900 ms, flip angle = 7°, FOV = 256 × 256 mm, slices = 176, resolution matrix = 256 × 256, voxel size = 1 × 1 × 1 mm^3, number of echos = 5, pixel bandwidth =650 Hz, total scan time = 6 min. With 5 echoes, the TR, TI and time to encode partitions for the MEMPR are similar to that of a conventional MPRAGE, resulting in similar GM/WM/CSF contrast.

Neuroimaging data from the different data sets were preprocessed independently using Statistical Parametric Mapping (SPM) and the Data Processing & Analysis of Brain Imaging toolbox (DPABI) (2, 14). The first 10 volumes were discarded to suppress the equilibration effects and consider subjects' adaptation to the environment. The remaining volumes were slice-timing corrected, realigned, and spatially normalized to the MNI (Montreal Neurological Institute) template and resampled to 3 × 3 × 3 mm^3. Nuisance signals including white matter, cerebrospinal fluid, and head motion parameters and their derivatives using the Friston 24-parameter model were regressed out to control the potential influence of physiological artifacts. We further implemented data scrubbing to better address head motion concerns. The bad time points were regressed that were defined as volumes with framewise displacement (FD) Power > 0.5 mm as well as the two succeeding volumes and one preceding volume to reduce the spillover effect of head motion (1). The

percentage of scrubbing volumes varied in the different datasets (BBP, mean=0.8%, SD=2.4%; SLIM, mean=1.2%, SD=2.7%; validation sample, mean=0.5%, SD=1.3%; generalized anxiety dataset, mean=8.4%, SD=10.6%; major depression dataset, mean=1.3%, SD=2.0%; schizophrenia dataset, mean=20.2%, SD=23.2%). For the concerns of excessive head motion during the brain scanning and to ensure that head motion artefacts were not driving observed effects, we adopted a widely used criterion to exclude participants based on > 10% bad volumes (1-3). We provide the flow diagram for details on participants' screening in Figure S1. In addition, linear trends were also included as regressors since the BOLD signal exhibits low-frequency drifts. We next conducted spatial smoothing with 4-mm full-width at half-maximum Gaussian kernel and band-pass temporal filtering (0.01–0.10 Hz). Finally, we did not perform global signal regression (GSR) for several reasons: the use of GSR has always been debated since the global signal also includes neuronal-related BOLD fluctuations, particularly if these are strong and widespread across the brain. If the global signal was removed, these neuronal-related fluctuations could also be removed. GSR introduces a negative bias in the estimated BOLD response, decreasing positive BOLD responses and artificially creating negative ones or "deactivations" (15-18). Similarly, the overall effect of GSR in measures of correlation is to force the average correlation across the brain to be zero (19). GSR may artificially introduce anti-correlations between brain regions, which would otherwise exhibit no significant correlations (19, 20).

Method S3. Functional Network Construction

For all data sets, the preprocessed data were parcellated into 246 regions of interest (ROIs) using the Human Brainnetome Atlas that includes 210 cortical and 36 subcortical ROIs (21). The representative time series of each node was obtained for each individual by averaging the time series over all of the voxels therein. The Pearson correlation of the time courses between each node pair was calculated and then a Fisher's z transformation was performed to improve normality, resulting in a 246 × 246 symmetric FC matrix with 30,135 unique edges for each participant. We

chose the Human Brainnetome Atlas because it provides a new framework for human brain research and in particular connectome analysis that integrates multimodal information and overcomes several drawbacks of previous parcellation schemes: 1) it establishes a priori, biologically valid brain parcellation scheme of the entire cortical and subcortical gray matter into subregions showing a coherent pattern of anatomical connections; 2) it provides detailed characterizations of the structural and functional connectivity patterns for these; and 3) it decodes brain functions by establishing those tasks and contrasts that activated the respective area above chance in previous task-based functional neuroimaging studies (21).

Method S4. Prediction Analysis

We applied three machine learning methods (i.e., relevance vector regression (RVR), support vector regression (SVR), and elastic-net regression) to examine the predictions from the functional connectome of individuals' daily anxiety and pandemic-related anxiety. The BBP was used to examine the predictions from the functional connectome of daily anxiety and pandemic-related anxiety (first pandemic survey). The SLIM was used to validate the predictions from the functional connectome of daily anxiety using the same predictive framework of machine learning.

RVR is a sparse kernel multivariate regression method that uses Bayesian inference to obtain parsimonious solutions that can generalize well and provide inferences at low computational cost (22). Compared to a support vector machine, the Bayesian formulation of the RVR avoids the set of free parameters of the SVR (that usually require cross-validation-based post-optimizations). Thus, we used the traditional 10-fold cross validation (10F-CV) rather than nested 10F-CV for RVR. All subjects of the BBP or SLIM were randomly divided into 10 subsets, 9 folds (90% subjects) were used as the training set, and the remaining one fold (10% subjects) were used as the testing set. Feature selection was performed in the training set by correlating anxiety score with the whole-brain FC using Pearson partial correlation (removing the confounding effects of sex, age, head motion, and baseline anxiety score), retaining

only important FCs with high correlation coefficient corresponding to a specific p value. Some research tended to choose a single threshold to select features (23). However, it is noted that there is often a lack of sufficient justification for choosing a specific single threshold. Recent studies suggest that multiple different thresholds would be useful in at least two ways (24-26). First, it is helpful to illustrate the comprehensive prediction performance by avoiding the the arbitrariness of a single threshold. Second, it is also helpful to explore the optimal prediction performance. Thus, we applied several common thresholds (uncorrected p values: 1×10^{-4}, 5×10^{-4}, 1×10^{-3}, 5×10^{-3}, 1×10^{-2}, 5×10^{-2}) for feature selection (24). To avoid features in greater numeric ranges dominating those in smaller numeric ranges, the selected features were linearly scaled to the range of 0 to 1 across the training set, and the scaling parameters were also applied to scale the testing set (27). A regression model was built using RVR to fit the selected FCs and anxiety scores in the training set. Next, the same FCs were extracted from the testing set and then fed into the RVR model to generate the predicted anxiety scores. After all folds were completed, we obtained the predicted scores for each participant. Since each random division results in a different testing set and training set, we repeated the above prediction pipeline 20 times to generate 20 predicted scores for each participant and further averaged these predicted scores to obtain robust estimates. Pearson correlation coefficients between the predicted and actual scores were computed to provide final estimate of prediction performance. We randomly shuffled the anxiety scores 1,000 times and ran the above prediction pipeline for each time to obtain a null distribution of correlation coefficient between the predicted and actual scores to estimate the significance.

To validate the robustness of the prediction results, two other machine learning linear regression algorithms, elastic-net regression and SVR were also applied. Elastic-net regression uses a weighted combination of ridge regression (L2 regularization) and least absolute shrinkage and selection operator (LASSO, L1 regularization) (28). The L2 regularization minimizes the sum of the squares of regression coefficients and retains all features in the model (29). The L1 regularization minimizes the sum of the absolute value of regression coefficients and

retains only a small set of features (i.e., the regression coefficients of many features equal zero) (28, 30). Thus, the LASSO will construct a sparse model by excluding the majority of features from the model, which helps to improve predictive performance and reduce the model complexity (31). However, the LASSO can only select *N*-1 features at most, where *N* is equal to the sample size (32), which may be problematic for a model with a large number of features but few samples (27). To overcome this limitation, elastic-net regression combines L1 and L2 regularization, which allows the number of the selected features to be larger than the sample size while achieving a sparse model (28). The regularization parameter λ shrinks the regression coefficients and controls the trade-off between the bias and variance. A large λ represents a greater penalty on model complexity (variance), and a small λ corresponds to a greater penalty on training error (bias). Another parameter α is used to control the relative weighting of the L1 and L2 regularization contributions (α = 0, ridge regression, L2 regularization; α = 1, LASSO, L1 regularization). We set the α value to 0.5 to take advantage of the relative strengths between ridge regression and LASSO, providing a non-sparse solution with low variance (33).

Also, linear SVR with a cost parameter (*C*) was applied to train the model (34-36). The parameter *C* controls the trade-off between the how strongly the samples that deviate by more than ε are tolerated and the flatness of the regression line, i.e., the trade-off of penalties between the bias and variance. A large *C* corresponds to more penalties on bias, and a small *C* corresponds to more penalties on variance (27).

To determine the optimal λ and *C* (searching in [0,1] with a step of 0.1), a nested 10F-CV was applied, with the outer 10F-CV loop estimating the generalizability of the model and the inner 10F-CV loop determining the optimal parameters (λ or *C*) for elastic-net regression and support vector regression (27) (Figure 1B). All subjects were randomly divided into 10 subsets, 9 folds (90% subjects) were used as the training set, and the remaining one fold (10% subjects) were used as the testing set. Feature selection and scaling procedure were the same as described in RVR section. The principal difference is that we applied inner 10F-CV within training set was used to determining the optimal parameters. Specifically, the training set was further

randomly divided into 10 subsets. Nine subsets were used to train the model under a given parameter λ (elastic-net regression) or *C* (SVR), and the remaining subset was used to test the model. This procedure was repeated 10 times such that each subset was used once as the testing set. The mean absolute error (MAE) were generated for each parameter. The parameter with the minimum MAE was chosen as the optimal parameter and applied to build the model using the whole training set. Accordingly, each loop of the outer 10F-CV yielded a specific optimal parameter. The outer testing set was then inputted into the model to generate the predictive score. Since each random division results in different testing set and training set, we repeated the above prediction pipeline 20 times to generate 20 predicted scores for each participant and further averaged these predicted scores to obtain robust estimates. The Pearson correlation coefficient between the predicted and actual scores were computed to provide final estimate of prediction performance. We randomly shuffled the anxiety scores 1,000 times and ran the above prediction pipeline for each time to obtain a null distribution of correlation coefficients between the predicted and actual scores to estimate the significance.

Method S5. Clinical Extension

Finally, we used binary logistic regression to examine whether the identified consensus FCs could be used to distinguish between specific mental disorders and the matched HCs. To overcome the overfitting problem that may be caused by a set of features, we applied a regularization technique to address this issue. The L1 regularization minimizes the sum of the absolute value of regression coefficients and retains only a small set of features (i.e., the regression coefficients of many features equal zero) to fit a sparse model (28). The L2 regularization minimizes the sum of the squares of regression coefficients and retains all features in the model (28). Since the consensus FCs have been selected from the above 10F-CV and there is no need to narrow it more, L2 regularization was applied in the following analysis. We applied nested 10F-CV, with outer 10F-CV estimating the generalizability of the model and the inner 10F-CV determining the optimal regularization parameter λ, which is

similar to the above regression prediction pipeline. The difference is that classification prediction does not need feature selection and the area under the receiver operating characteristic curve (AUC) assesses the prediction performance to determine the optimal parameter. Since each random division results in a different testing set and training set, we repeated the nested 10F-CV 20 times and averaged classification performance across the 20 times to generate the overall prediction accuracy. We performed two types of permutation test to ensure that the classification results were significantly better than random. For the first type of permutation test (pt1), we retained the consensus FCs but randomly shuffled the diagnostic label 1,000 times and ran the prediction pipeline to obtain a null distribution of classification performance. For the second type of permutation test (pt2), we retained the diagnostic label but randomly selected the same number of consensus FCs 1,000 times and ran the prediction pipeline to obtain a null distribution of classification performance.

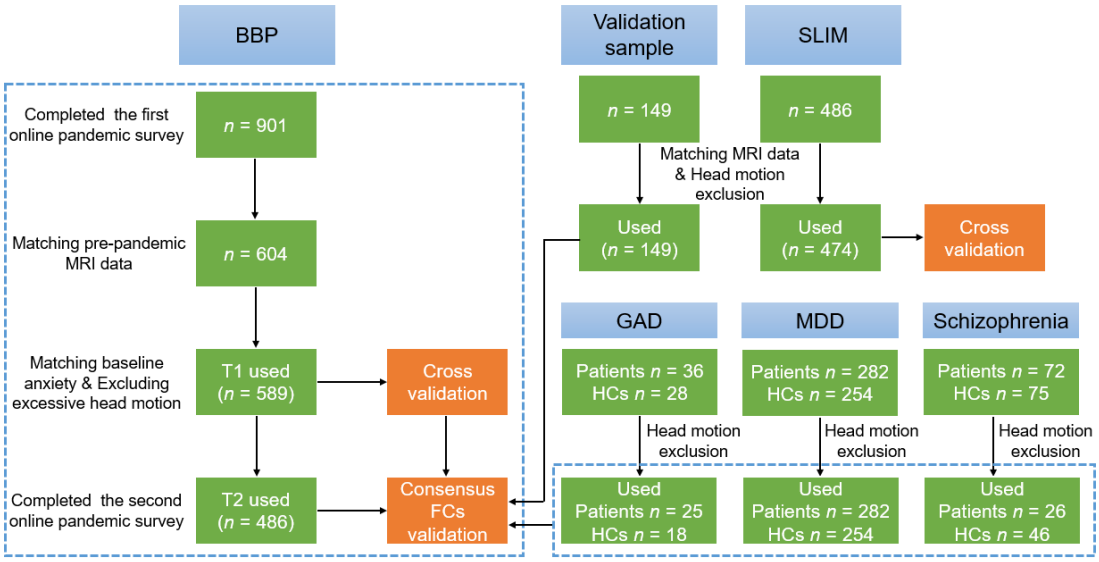

Figure S1. The flow diagram of participants' screening. BBP=Behavioural Brain Research Project of Chinese Personality; GAD=generalized anxiety disorder dataset; MDD=major depression disorder dataset; SLIM= Southwest University Longitudinal Imaging Multimodal Project; HCs=healthy controls.

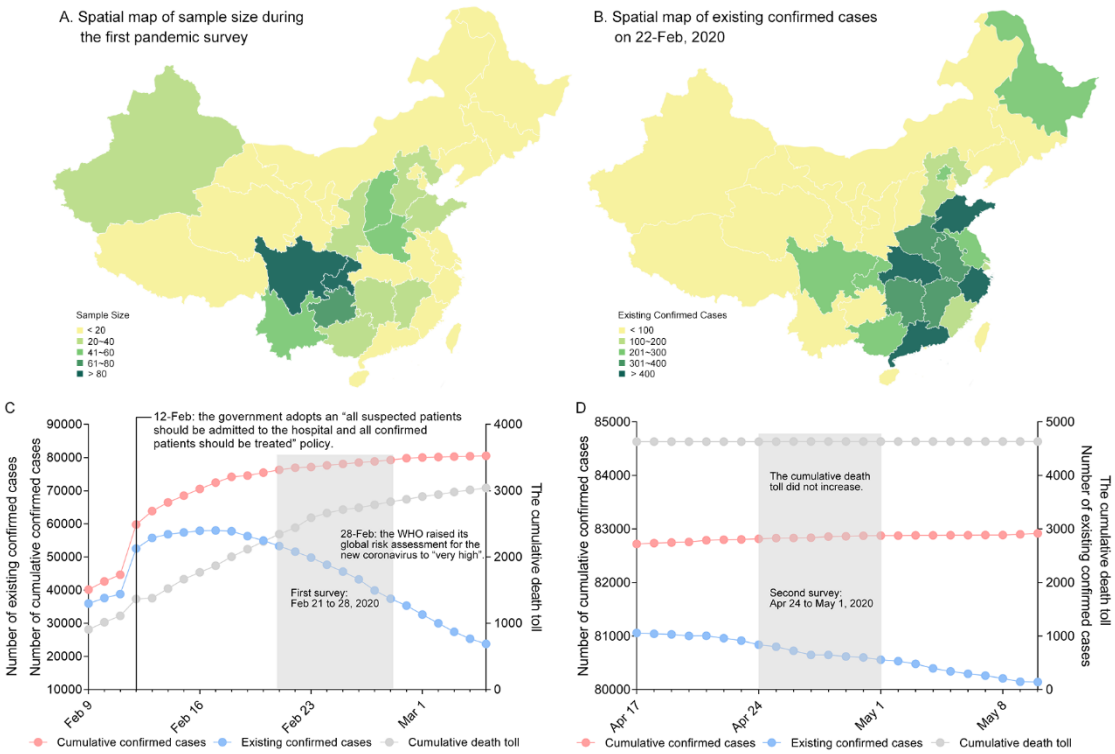

Figure S2. The spatial map of sample size and COVID-19 case information during our pandemic survey in China. (A) The spatial map of sample size during the first pandemic survey. (B) The spatial map of existing confirmed cases on February 22, 2020. (C) The first online questionnaire survey was conducted from February 21 to 28, 2020 and the number of existing confirmed cases ranged from 39,919 to 54,965. (D) The second online questionnaire survey was conducted from April 24 to May 1, 2020, and the number of existing confirmed cases was ranged from 557 to 838.

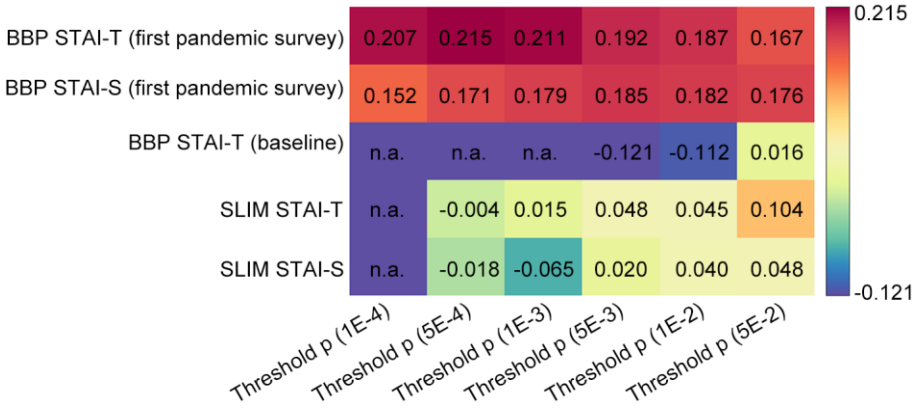

Figure S3. Prediction results of the relevance vector regression. Each square represents the Pearson correlation between the predicted and measured anxiety score. The first two rows show that the prediction from the functional connectome of pandemic-related anxiety was better than random (permutation test, all $p<0.05$). The last three rows show that the prediction from the functional connectome on daily anxiety was not significantly higher than random (permutation test, all $p>0.05$). "n.a." indicates that prediction results are unavailable. Due to the weak correlation between daily anxiety and the whole-brain functional connectivity, no functional connectivity was selected in the training set at a low threshold and then the regression model cannot be built, thus the predicted anxiety score cannot be obtained. BBP= Behavioural Brain Research Project of Chinese Personality; SLIM=Southwest University Longitudinal Imaging Multimodal Project; STAI-T=the trait section of the State-Trait Anxiety Inventory; STAI-S=the state section of the State-Trait Anxiety Inventory.

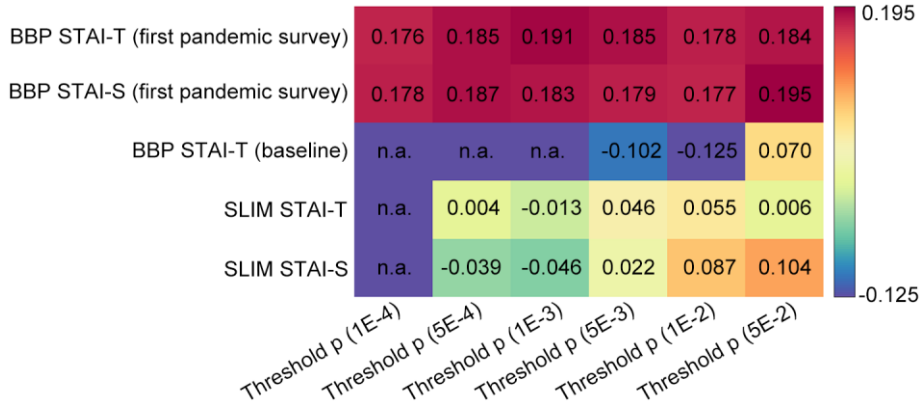

Figure S4. Prediction results of the elastic-net regression. Each square represents the Pearson correlation between the predicted and measured anxiety score. The first two rows show that the prediction from the functional connectome of pandemic-related anxiety was better than random (permutation test, all $p<0.05$). The last three rows show that the prediction from the functional connectome of daily anxiety was not significantly higher than random (permutation test, all $p>0.05$). "n.a." indicates that prediction results are unavailable. Due to the weak correlation between daily anxiety and the whole-brain functional connectivity, no functional connectivity was selected in the training set at a low threshold and then the regression model cannot be built, thus the predicted anxiety score cannot be obtained. BBP=Behavioural Brain Research Project of Chinese Personality; SLIM=Southwest University Longitudinal Imaging Multimodal Project; STAI-T=the trait section of the State-Trait Anxiety Inventory; STAI-S=the state section of the State-Trait Anxiety Inventory.

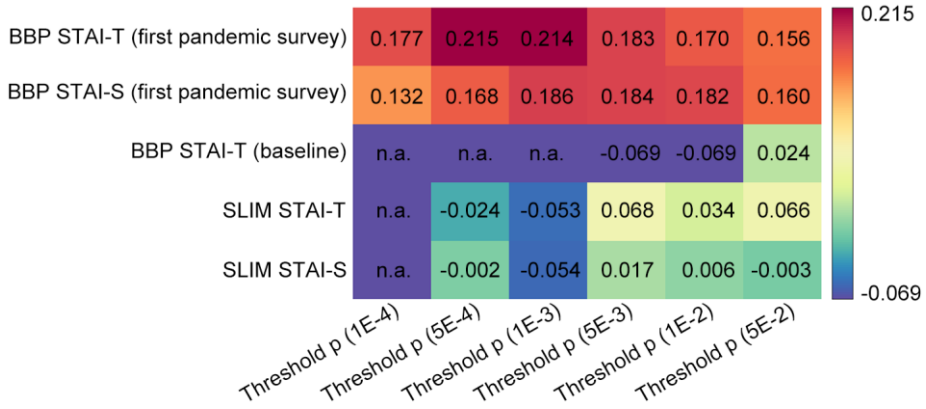

Figure S5. Prediction results of the support vector regression. Each square represents the Pearson correlation between the predicted and measured anxiety score. The first two rows show that the prediction from the functional connectome of pandemic-related anxiety was better than random (permutation test, all $p<0.05$). The last three rows show that the prediction from the functional connectome of daily anxiety was not significantly higher than random (permutation test, all $p>0.05$). "n.a." indicates that prediction results are unavailable. Due to the weak correlation between daily anxiety and the whole-brain functional connectivity, no functional connectivity was selected in the training set at a low threshold and then the regression model cannot be built, thus the predicted anxiety score cannot be obtained. BBP= Behavioural Brain Research Project of Chinese Personality; SLIM=Southwest University Longitudinal Imaging Multimodal Project; STAI-T=the trait section of the State-Trait Anxiety Inventory; STAI-S=the state section of the State-Trait Anxiety Inventory.

Table S1. Demographic characteristics for the three undergraduate datasets

Comparison (Group1 vs Group 2)	Gender (M/F)			Age (Mean)			Age (SD)	
	Group1	Group2	p^a	Group1	Group2	p^b	Group1	Group2
BBP vs SLIM	173/416	207/267	<0.05	19.35	20.02	<0.05	0.87	1.28
BBP vs Validation Sample	173/416	22/127	<0.05	19.35	19.25	<0.05	0.87	0.62
SLIM vs Validation Sample	207/267	22/127	<0.05	20.02	19.25	>0.05	1.28	0.62

Note. a, χ^2 test; b, two sample *t*-test; two-tailed. SD=standard deviation; BBP=Behavioural Brain Research Project of Chinese Personality; SLIM=Southwest University Longitudinal Imaging Multimodal Project.

Table S2. Demographic characteristics for the three clinical datasets

Dataset	Number		Gender (M/F)			Age (Mean)			Age (SD)	
	Patient	HC	Patient	HC	p^a	Patient	HC	p^b	Patient	HC
Generalized anxiety	25	18	10/15	9/9	>0.05	16.84	16.72	>0.05	0.47	0.89
Major depression	282	254	99/183	88/166	>0.05	38.74	39.65	>0.05	13.65	15.80
Schizophrenia	26	46	22/4	33/13	>0.05	31.92	32.65	>0.05	12.35	10.67

Note. a, χ^2 test; b, two sample *t*-test; two-tailed. SD=standard deviation.

Table S3. The Pearson partial correlation between the consensus functional connectivity and pandemic-related anxiety

Node 1	MNI (x, y, z)			Node 2	MNI (x, y, z)			r[a]	p	p (FDR corrected)
L. dorsolateral SFG	-18	24	53	R. Postcentral Gyrus	55	-10	15	-0.205	6.53E-07	3.97E-03
L. medial SFG	-6	-6	58	L. dorsal dysgranular insula	-38	6	4	-0.203	8.14E-07	3.97E-03
L. medial SFG	-6	-6	58	L. occipital thalamus	-14	-28	4	-0.192	3.15E-06	3.97E-03
R. medial SFG	7	-4	60	R. caudal temporal thalamus	10	-14	14	-0.188	5.10E-06	4.14E-03
L. inferior frontal junction	-42	14	36	R. pregenual Cingulate Gyrus	5	28	28	-0.192	3.10E-06	3.97E-03
L. inferior frontal junction	-42	14	36	L. ventromedial putamen	-22	7	-4	-0.194	2.51E-06	3.97E-03
L. ventrolateral MFG	-32	4	54	R. hypergranular insula	37	-18	8	-0.197	1.81E-06	3.97E-03
L. ventrolateral MFG	-32	4	54	L. ventromedial putamen	-22	7	-4	-0.190	4.32E-06	4.14E-03
L. dorsal IFG	-46	13	23	R. Postcentral Gyrus	55	-10	15	-0.191	3.82E-06	3.97E-03
L. dorsal IFG	-46	13	23	R. hypergranular insula	37	-18	8	-0.202	9.82E-07	3.97E-03
L. Precentral Gyrus	-49	-7	39	R. Parahippocampal Gyrus	18	-9	-30	-0.202	9.64E-07	3.97E-03
L. Precentral Gyrus	-32	-9	58	L. occipital thalamus	-14	-28	4	-0.206	6.04E-07	3.97E-03
L. Precentral Gyrus	-49	5	30	R. Parahippocampal Gyrus	18	-9	-30	-0.192	3.08E-06	3.97E-03
L. Precentral Gyrus	-49	5	30	R. rostroventral Cingulate Gyrus	4	22	12	-0.198	1.67E-06	3.97E-03
L. Precentral Gyrus	-49	5	30	L. sensory thalamus	-18	-23	3	-0.200	1.21E-06	3.97E-03
L. Paracentral Lobule	-4	-23	61	L. dorsal dysgranular insula	-38	6	4	-0.189	4.88E-06	4.14E-03
L. STG	-53	-32	13	R. hypergranular insula	37	-18	8	-0.192	3.42E-06	3.97E-03
R. caudal PhG	27	-22	-27	R. dorsal agranular insula	36	19	1	-0.193	2.95E-06	3.97E-03
R. caudal PhG	27	-22	-27	R. posterior parietal thalamus	17	-26	6	-0.196	2.03E-06	3.97E-03
L. posterior PhG	-28	-33	-17	L. occipital thalamus	-14	-28	4	-0.184	8.74E-06	4.14E-03
R. SPL	23	-44	67	L. lateral pre-frontal thalamus	-11	-14	3	-0.192	3.31E-06	3.97E-03
L. intraparietal SPL	-28	-59	54	R. hypergranular insula	37	-18	8	-0.191	3.52E-06	3.97E-03
L. rostrodorsal IPL	-38	-61	46	R. Postcentral Gyrus	55	-10	15	-0.183	8.85E-06	4.14E-03
L. rostrodorsal IPL	-38	-61	46	R. hypergranular insula	37	-18	8	-0.194	2.50E-06	3.97E-03
L. medial Precuneus	-8	-47	57	R. posterior parietal thalamus	17	-26	6	-0.180	1.25E-05	4.14E-03
L. Postcentral Gyrus	-46	-30	50	L. sensory thalamus	-18	-23	3	-0.223	5.77E-08	1.74E-03
R. Postcentral Gyrus	47	-25	48	L. sensory thalamus	-18	-23	3	-0.212	2.66E-07	3.97E-03
R. hypergranular insula	37	-18	8	L. rostral hippocampus	-22	-13	-20	-0.194	2.70E-06	3.97E-03
R. hypergranular insula	37	-18	8	R. sensory thalamus	18	-22	3	-0.191	3.59E-06	3.97E-03
R. hypergranular insula	37	-18	8	R. posterior parietal thalamus	17	-26	6	-0.198	1.64E-06	3.97E-03
L. rostral hippocampus	-22	-13	-20	R. globus pallidus	22	-3	3	-0.196	1.96E-06	3.97E-03
L. dorsolateral putamen	-28	-5	2	L. sensory thalamus	-18	-23	3	-0.184	8.48E-06	4.14E-03

Note. a, the Pearson partial correlation coefficients between the consensus FCs and STAI-T score (first pandemic survey) ranged from -0.223 to -0.180 after controlling for sex, age, head motion, and baseline anxiety. The template information was extracted from the Human Brainnetome Atlas (21). L=left hemisphere; R=right hemisphere.

References

1. Power JD, Barnes KA, Snyder AZ, Schlaggar BL, Petersen SE. Spurious but systematic correlations in functional connectivity MRI networks arise from subject motion. NeuroImage. 2012;59(3):2142-54.
2. Yan C-G, Wang X-D, Zuo X-N, Zang Y-F. DPABI: Data Processing & Analysis for (Resting-State) Brain Imaging. Neuroinformatics. 2016;14(3):339-51.
3. Cheng W, Rolls ET, Qiu J, Liu W, Tang Y, Huang C-C, et al. Medial reward and lateral non-reward orbitofrontal cortex circuits change in opposite directions in depression. Brain. 2016;139(12):3296-309.
4. Liu W, Wei D, Chen Q, Yang W, Meng J, Wu G, et al. Longitudinal test-retest neuroimaging data from healthy young adults in southwest China. Scientific Data. 2017;4.
5. Spielberger CD. State-Trait Anxiety Inventory. In: Weiner IB, Craighead WE, editors. The Corsini Encyclopedia of Psychology2010.
6. Yan C-G, Chen X, Li L, Castellanos FX, Bai T-J, Bo Q-J, et al. Reduced default mode network functional connectivity in patients with recurrent major depressive disorder. Proc Natl Acad Sci U S A. 2019;116(18):9078-83.
7. Yang F, Fan L, Zhai T, Lin Y, Wang Y, Ma J, et al. Decreased Intrinsic Functional Connectivity in First-Episode, Drug-Naive Adolescents With Generalized Anxiety Disorder. Front Hum Neurosci. 2019;12(539).
8. Gifford G, Crossley N, Kempton MJ, Morgan S, Dazzan P, Young J, et al. Resting state fMRI based multilayer network configuration in patients with schizophrenia. NeuroImage: Clinical. 2020;25:102169.
9. Yang F, Zhang J, Fan L, Liao M, Wang Y, Chen C, et al. White matter structural network disturbances in first-episode, drug-naïve adolescents with generalized anxiety disorder. J Psychiatr Res. 2020;130:394-404.
10. Birmaher B, Brent DA, Chiappetta L, Bridge J, Monga S, Baugher M. Psychometric Properties of the Screen for Child Anxiety Related Emotional Disorders (SCARED): A Replication Study. J Am Acad Child Adolesc Psychiatry. 1999;38(10):1230-6.
11. Su L, Wang K, Fan F, Su Y, Gao X. Reliability and validity of the screen for child anxiety related emotional disorders (SCARED) in Chinese children. J Anxiety Disord. 2008;22(4):612-21.
12. Kaufman J, Birmaher B, Brent D, Rao UMA, Flynn C, Moreci P, et al. Schedule for Affective Disorders and Schizophrenia for School-Age Children-Present and Lifetime Version (K-SADS-PL): Initial Reliability and Validity Data. J Am Acad Child Adolesc Psychiatry. 1997;36(7):980-8.
13. Axelrod BN. Validity of the Wechsler Abbreviated Scale of Intelligence and Other Very Short Forms of Estimating Intellectual Functioning. Assessment. 2002;9(1):17-23.
14. Yan C-G, Zang Y-F. DPARSF: A MATLAB Toolbox for "Pipeline" Data Analysis of Resting-State fMRI. Front Syst Neurosci. 2010;4(1):1-13.
15. Desjardins AE, Kiehl KA, Liddle PF. Removal of Confounding Effects of Global Signal in Functional MRI Analyses. NeuroImage. 2001;13(4):751-8.

16. Gavrilescu M, Shaw ME, Stuart GW, Eckersley P, Svalbe ID, Egan GF. Simulation of the Effects of Global Normalization Procedures in Functional MRI. NeuroImage. 2002;17(2):532-42.
17. Junghöfer M, Schupp HT, Stark R, Vaitl D. Neuroimaging of emotion: empirical effects of proportional global signal scaling in fMRI data analysis. NeuroImage. 2005;25(2):520-6.
18. Macey PM, Macey KE, Kumar R, Harper RM. A method for removal of global effects from fMRI time series. NeuroImage. 2004;22(1):360-6.
19. Murphy K, Birn RM, Handwerker DA, Jones TB, Bandettini PA. The impact of global signal regression on resting state correlations: Are anti-correlated networks introduced? NeuroImage. 2009;44(3):893-905.
20. Weissenbacher A, Kasess C, Gerstl F, Lanzenberger R, Moser E, Windischberger C. Correlations and anticorrelations in resting-state functional connectivity MRI: A quantitative comparison of preprocessing strategies. NeuroImage. 2009;47(4):1408-16.
21. Fan L, Li H, Zhuo J, Zhang Y, Wang J, Chen L, et al. The Human Brainnetome Atlas: A New Brain Atlas Based on Connectional Architecture. Cereb Cortex. 2016;26(8):3508-26.
22. Tipping ME. Sparse Bayesian learning and the relevance vector machine. Journal of Machine Learning Research. 2001;1(3):211-44.
23. Feng C, Wang L, Li T, Xu P. Connectome-based individualized prediction of loneliness. Soc Cogn Affect Neurosci. 2019;14(4):353-65.
24. Shen X, Finn ES, Scheinost D, Rosenberg MD, Chun MM, Papademetris X, et al. Using connectome-based predictive modeling to predict individual behavior from brain connectivity. Nat Protoc. 2017;12(3):506-18.
25. Greene AS, Gao S, Scheinost D, Constable RT. Task-induced brain state manipulation improves prediction of individual traits. Nature Communications. 2018;9(1):2807.
26. Jiang R, Calhoun VD, Zuo N, Lin D, Li J, Fan L, et al. Connectome-based individualized prediction of temperament trait scores. NeuroImage. 2018;183:366-74.
27. Cui Z, Gong G. The effect of machine learning regression algorithms and sample size on individualized behavioral prediction with functional connectivity features. NeuroImage. 2018;178:622-37.
28. Zou H, Hastie T. Regularization and variable selection via the elastic net. Journal of the Royal Statistical Society Series B-Statistical Methodology. 2005;67:301-20.
29. Hoerl AE, Kennard RW. RIDGE REGRESSION - BIASED ESTIMATION FOR NONORTHOGONAL PROBLEMS. Technometrics. 1970;12(1):55-&.
30. Tibshirani R. Regression shrinkage and selection via the Lasso. Journal of the Royal Statistical Society Series B-Methodological. 1996;58(1):267-88.
31. Wright J, Ma Y, Mairal J, Sapiro G, Huang TS, Yan S. Sparse Representation for Computer Vision and Pattern Recognition. Proceedings of the Ieee. 2010;98(6):1031-44.
32. Ryali S, Chen T, Supekar K, Menon V. Estimation of functional connectivity in fMRI data using stability selection-based sparse partial correlation with elastic net penalty. NeuroImage. 2012;59(4):3852-61.

33. Pedersen M, Zalesky A, Omidvarnia A, Jackson GD. Multilayer network switching rate predicts brain performance. Proc Natl Acad Sci U S A. 2018;115(52):13376-81.
34. Vapnik V. The Nature of Statistical Learning Theory. New York: Springer-Verlag; 2000.
35. Smola AJ, Scholkopf B. A tutorial on support vector regression. StCom. 2004;14(3):199-222.
36. Chang C-C, Lin C-J. LIBSVM: A library for support vector machines. ACM transactions on intelligent systems and technology. 2011;2(3):27.